


Hydrothermal Dissolution of Technical Grade Vitreous Silica in NaOH Solutions to Liquid Water Glasses with Higher SiO₂:Na₂O Ratios

Thomas Pfeiffer^{1,2}, Dirk Enke³, and Hans Roggendorf^{1,*}

DOI: 10.1002/cite.202000107

 This is an open access article under the terms of the Creative Commons Attribution-NonCommercial-NoDerivs License, which permits use and distribution in any medium, provided the original work is properly cited, the use is non-commercial and no modifications or adaptations are made.



Supporting Information
available online

Technical grade vitreous silica was dissolved hydrothermally in NaOH lyes. Liquid sodium water glasses with silica concentrations of up to 26.4 wt % and molar SiO₂:Na₂O ratios of up to 3.5 were obtained. The dissolution behavior showed two temperature regimes: up to 130 °C the SiO₂ content approached a final solubility limit controlled by cristobalite crystallization. Above 130 °C, crystallization of low quartz restricted solubility. The dissolution kinetics were governed by surface area reduction and saturation control according to the Noyce-Whitney law.

Keywords: Hydrothermal dissolution, Solubility, Vitreous silica, Water glass

Received: May 25, 2020; *accepted:* December 07, 2020

1 Introduction

Commercially available liquid sodium water glasses have compositions characterized by molar SiO₂:Na₂O ratios (R_m) values between 1.8 and 4 (ratios of 2.0 and 3.3 are standard compositions) and silica contents of 25 to 35 wt %. Weldes [1] reported that R_m values up to 2.7 were reached by hydrothermal dissolution of quartz sands in sodium hydroxide lyes, usually at temperatures up to 200 °C. Typical conditions were specified in [2]. Reports on the application of raw materials with a higher reactivity – like cristobalite or vitreous silica – in order to reach higher R_m values are published in the patent literature (e.g., [3]). Studies on dissolution of opal and low quartz materials to synthesize liquid sodium water glass were presented in [4, 5].

The solubility of silica in general was already treated in [5] and the solubility of low quartz in [4]. In the present report, the literature concerning and dissolution kinetics of vitreous silica is evaluated. Generally, the solubility of silica increases with pH and temperature.

At neutral conditions (pH about 8.4) Iler [6] refers to the work of Stöber [7] that the equilibrium concentration of (Si(OH)₄), which limits the solubility at this pH, decreases in the order

vitreous silica > stishovite > cristobalite >
tridymite > quartz > coesite (1)

In pure water, vitreous silica reaches a solubility of 1500 ppm at 350 °C (Gunnarsson et al. [8]). At alkaline pH values higher solubilities up to the concentration range of commercial liquid sodium water glass compositions are reported due to the formation of negatively charged silicate ions and silicate colloids [9].

Rimstidt and Barnes [10] investigated silica-water reactions at higher temperatures with special respect to geological conditions. They report that the solubility of the respective phases increases under these conditions in the order

amorphous silica > β–cristobalite > α–cristobalite > quartz (2)

They correlate this solubility dependence with the free enthalpy of formation of the silica phases. With respect to dissolution behavior, amorphous silica and cristobalite are thermodynamically less stable than low quartz in the

¹Thomas Pfeiffer, Prof. Dr.-Ing. Hans Roggendorf

hans.roggendorf@physik.uni-halle.de

Martin-Luther-University Halle-Wittenberg, Institute of Physics, Von-Danckelmann-Platz 3, 06120 Halle (Saale), Germany.

²Thomas Pfeiffer

OPTERRA Zement GmbH, Straße der Einheit, 06638 Karsdorf, Germany.

³Prof. Dr. rer. nat. Dirk Enke

University of Leipzig, Institute of Chemical Technology, Linnéstraße 3, 04103 Leipzig, Germany.

temperature range between room temperature and 250 °C [6]. It has to be mentioned here that the term amorphous silica may denote different materials, dense vitreous silica as well as finely dispersed varieties such as silica gel or even leached porous glass of the Vycor™ type.

Higher pH values require alkalis or organic hydroxides as part of the solvent. Iler [6] and Stumm [11] used thermodynamic data to calculate equilibrium solubilities of low quartz and amorphous silica (not specified here) involving the neutral molecule $\text{Si}(\text{OH})_4(\text{aq.})$ as well as negatively charged silicate anions like $\text{HSiO}_3^-(\text{aq.})$ and $\text{SiO}_3^{2-}(\text{aq.})$ as a function of pH at 25 °C. Above pH 9 the solubility of both silica phases increases due to the formation of these silicate anions. At all pH values above pH 7, the solubility of amorphous silica is by a factor of 10 higher than that of low quartz. Thus, amorphous silica reaches solubilities of up to 10 mol L^{-1} .

Falcone et al. [9] confirmed the data of Stumm et al. [11]. They differentiated a stable mononuclear region with only monomeric molecules and anions in solution, a stable multimeric domain with oligomeric and colloidal silica, and an insoluble domain, where the precipitation of silica is observed. The existence of colloids is generally excepted (Andersson et al. [12], Iler [13], Böschel et al. [14]), they are supposed to be stabilized by an electrostatic double layer creating repulsive forces. This is basically described by the DLVO theory named after Derjaguin, Landau, Verweij and Overbeek [15] but some details concerning its application to silica sols are still discussed (e.g., Haley [16], Bitter [17]).

The dissolution of silica in neutral or weakly alkaline solutions is often treated as first order reaction with a dissolution rate depending on concentration. According to Rimstidt and Barnes [10] the kinetics of silica dissolution at neutral conditions is controlled by an activated transition state governing the forward and backward reactions (3):



Dove and Crerar [18] applied the same first order reaction rate law to various silica sources and reported activation energies between 60 and 94 kJ mol^{-1} , some of them from literature data. Their own results ranged between 75 and 83 kJ mol^{-1} for various types of amorphous silica.

With opal as starting material, liquid sodium water glasses with SiO_2 contents up to 27 wt % and R_m values of 3.4 were obtained at intermediate dissolution times [5]. At longer dissolution times the silica concentrations decreased to about 22 wt % in a way resembling a LaMer-type [19] dissolution behavior. Seeding with microcrystalline silica phases like tridymite or low quartz possibly induced the solubility decrease at longer dissolution times. The use of low quartz resulted in silica solubilities of about 20 wt % nearly independent of temperature between 100 and 220 °C. R_m values of about 2.5 were reached [4]. The results confirmed a first order kinetics where the dissolution rate is controlled by the surface area and the concentration of silica according

to the relation established by Noyce and Whitney [20]. The proposed mathematical model allowed separating effects of surface area and SiO_2 concentration. Thus, temperature-dependent initial dissolution rates were calculated, which yielded an activation energy of $75 \pm 5 \text{ kJ mol}^{-1}$. A transient supersaturation was not observed.

The results reported here focus on the hydrothermal production of water glass by dissolving vitreous silica in NaOH brines at temperatures between 100 and 220 °C. A commercially available quality of vitreous silica was used to test the applicability of this process for larger scale manufacturing. The investigations aimed at a water glass composition with $R_m = 3.3$ and a silica content of 25 wt %. The kinetics of the dissolution process, concentration limitations of the obtained water glasses and the causes for them as well as interactions of kinetics and thermodynamics will be discussed.

2 Experimental

2.1 Raw Materials

QP-DN-50 of Saint Gobain Quartz, France, was applied as silica source. It is a technical grade vitreous silica powder with particle sizes below $100 \mu\text{m}$ ($d_{50} = 10 \mu\text{m}$) and a high purity ($\text{SiO}_2 \geq 99.8 \text{ wt } \%$). Dörentrup W6 (Dörentrup Quarz, Dörentrup, German, low quartz, $\text{SiO}_2 \geq 99.5 \text{ wt } \%$, $d_{50} = 9 \mu\text{m}$) was used for additional seeding. The NaOH lye (Akzo Nobel, Base Chemicals GmbH, Germany) had a nominal content of 50 wt % NaOH. By titration with HCl a value of 49.8 wt % NaOH was verified. Deionized H_2O was used for dilution. The electrical conductivity of the deionized H_2O was $< 5 \mu\text{S}$.

Vitreous silica was characterized by the following methods:

- The particle size distributions of the vitreous silica powders were analyzed by laser granulometry (CILAS 920, Quantachrome, Germany).
- The structure of vitreous silica was also characterized by XRD (URD 63, FPM Freiberg, Freiberg, Germany; $\text{CuK}\alpha$ radiation).
- The density was measured by He pycnometry (Pycnomatic ATC, Thermo Fisher Scientific Corp., Waltham, MA, USA).

2.2 Dissolution Method

The vitreous silica powders were dispersed in NaOH solutions and heat treated in autoclaves. Two different types of digestion bombs were used, each with a volume of 125 mL: PTFE (polytetrafluoroethylene)-lined steel bombs (type: Parr acid digestion bomb, Bomb No. 4748, company: Parr Instrument GmbH, Frankfurt, Germany) for temperatures $\geq 160 \text{ }^\circ\text{C}$ and PFA (perfluoro alkoxy alkanes) vessels (Savillex, Eden Prairie, Mn., USA) for temperatures of 100 and

130 °C. The digestion vessels were mounted in a rotating wheel inside a modified cabinet dryer (WTB ED 53, Binder, Germany). The temperature was controlled with a NiCr-Ni thermocouple and the mean temperature was kept within ± 2 K (short time variation due to temperature control of ± 5 K were possible) The rotation speed of the bombs was 25 rpm. Dissolution temperatures between 100 °C and 220 °C were applied and the dissolution times usually ranged from 1 h to 7 d (in a few cases dissolution times of 28 d were used). The experiments started at room temperature and ended by rapid cooling down by a forced cool air flow inside the drying cabinet. The dissolution time was corrected with respect to a dead time which is due to lower reactivity during heating and cooling. The dead times ranged between 25 and 90 min, depending on temperature, and were determined by evaluation of time-dependent dissolution runs.

2.3 Batch

Usually, batches of 40 g (quartz and NaOH brine) were applied. Their composition is listed in Tab. 1. Type A batches contained 25 wt % SiO₂ and 7.75 wt % Na₂O (the rest being H₂O), which corresponds to a molar ratio Si₂O:Na₂O (R_m) = 3.33. Here the batch composition is identical with the intended sodium water glass composition. Since nearly the whole silica content of batch A was dissolved in some dissolution tests the silica content was slightly increased. Two batches, B and C, contained an excess of silica compared to batch A: B had an excess of 5 % in comparison to A with R_m = 3.3, C had an excess of 10 %. Higher silica excesses than 10 %, however, led to gel like materials, which could not be separated into a liquid and a solid phase. The analysis of the dissolution data led to the conclusion that seeding has some influence on the kinetics. One hypothesis was that the residual low quartz found in the vitreous silica might be responsible for that. Therefore, batch D contained an additional amount of crystalline low quartz.

Table 1. Batch contents for the synthesis of liquid sodium water glasses with vitreous silica; H₂O content: 21.92 g; NaOH lye with 49.8 wt % NaOH: 8.08 g.

Batch	QP-DN50 [g]	W6 [g]
A	10	0
B	10.5	0
C	11	0
D	10.8	0.2

After cooling to room temperature, a liquid phase and a precipitate were separated by vacuum filtration. Pressures between 30 and 50 kPa were applied for nearly quantitative separation without significant evaporation of H₂O. A possible reduction of water content by that procedure was tested.

The results were reported in [4]. The additional error of SiO₂ analysis was < 0.2 wt %.

2.4 Analysis of the Liquid Phase and the Precipitates

An aliquot of the liquid phase was titrated with 0.5 mol L⁻¹ hydrochloric acid to analyze the alkali content (as Na₂O) of the solutions. Another aliquot of the liquid phase was calcined to determine the residual solids content (RSC). The samples were mixed with calcined quartz sand in order to avoid explosive steam emission during heating. Then the mixture was heated stepwise via 100 °C (heating rate 4 K min⁻¹) and 400 °C (4 K min⁻¹) to 900 °C (6 K min⁻¹) with holding times of 2 h at each temperature. Finally, the samples were cooled down to room temperature by switching off the furnace. The difference (RSC - Na₂O content) is equal to the SiO₂ content of the solution if impurities can be neglected (Al₂O₃ content of QP-DN50 \leq 0.2 wt %). R_m values were calculated from the analytical data.

The obtained liquids were characterized by the following methods: Density (pycnometry). Viscosity η (Brookfield viscosimeter DV2T, Middleboro, Ma., USA) and refractive index n (Abbe refractometer) were determined for selected samples. The precipitates were washed with deionized H₂O to remove alkalis which might react with CO₂ and dried gently at 30 °C. Then some of them were characterized by XRD (URD 63, FPM Freiberg, Freiberg, Germany; CuK α radiation).

3 Results

3.1 Raw Materials

The particle size distribution of QP-DN50 is listed in Tab. S1 in the Supporting Information (SI). The data will be used for modeling the dissolution behavior. Density of QP-DN50 was 2.259 ± 0.001 g cm⁻³. Brückner reported densities between 2.200 and 2.206 g cm⁻³ depending on type and fictive temperature of the specific vitreous silica [21]. The density measured here is slightly above the literature values, possibly due to phases or X-ray amorphous nanostructures with higher density. The densities of these phases are compared by Polyakova [22]:

- low quartz: 2.655 g cm⁻³,
- tridymite: 2.25–2.27 g cm⁻³,
- cristobalite: 2.32 g cm⁻³.

The XRD spectrogram of QP-DN50 is displayed in Fig. 1. The typical glass halo is present. Additionally, sharp peaks typical of crystalline phases can be seen. The strongest peak at $2\theta = 26.6^\circ$ [(101) or (011)] is typical for low quartz (RRUFF data base [23]: R110108) [24]. Smaller peaks at $2\theta = 39.5^\circ$ [(012) or (102)] and at $2\theta = 50.2^\circ$ [(112)] can also be attributed to low quartz. A comparison of peak areas

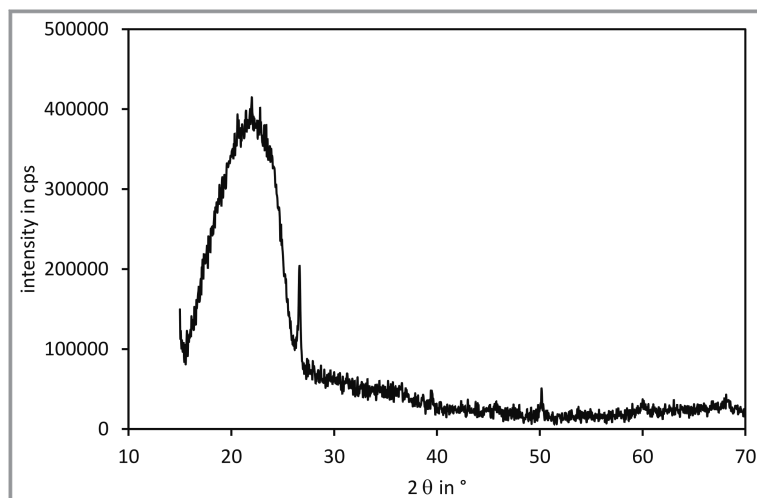


Figure 1. XRD spectrum of QP-DN50 vitreous silica, $\lambda(\text{CuK}\alpha) = 0.15418 \text{ nm}$; (RRUFF data base [23]: R110108).

showed that about 0.2 wt % might be crystalline low quartz, which is of course not a very reliable number. The strongest peak of cristobalite would appear at $2\theta = 22.0^\circ$ (RRUFF data base [23]: R060648). At that diffraction angle no peak was identified.

3.2 Dissolution Tests

The liquid sodium water glasses obtained by hydrothermal dissolution of batches containing vitreous silica QP-DN-50 were chemically analyzed. The Na_2O and SiO_2 contents are listed in Tab. S2 (SI). Some test runs failed, others were repeated. Liquid sodium water glasses with SiO_2 contents up to 26.4 wt % and R_m values up to 3.5 were reached. The developments of SiO_2 contents with dissolution time at selected temperatures are shown in Figs 2–4. The accuracy of the measurement was $\pm 0.2 \text{ wt } \%$ SiO_2 .

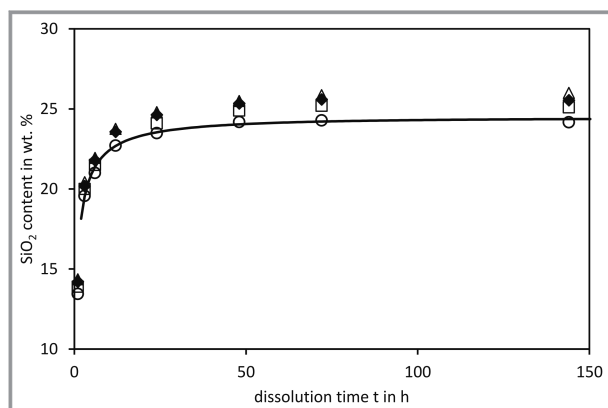


Figure 2. SiO_2 content of liquid water glass produced by hydrothermal dissolution at 100°C as a function of dissolution time t . \circ batch A; \square batch B; \triangle batch C; \blacklozenge batch D; — fit to batch A according to numerical simulation in [4]; results for batches C and D are nearly identical.

At 100°C (Fig. 2) and at 130°C the SiO_2 contents of the liquid sodium water glasses approached final values of about 25 wt %. At 160°C (Fig. 3) and 200°C (Fig. 4) the silica contents passed through a maximum, declined then with dissolution time, and approached a long-term limit of about 20 wt % SiO_2 . At 220°C the maximum SiO_2 content was already reached after 1 h of dissolution time and only the decline to a long-term limit of about 20 wt % SiO_2 was observed within the time range of the dissolution tests.

3.3 Materials Characterization

The concentration development of dissolution tests with batches containing vitreous silica at temperatures $\geq 160^\circ\text{C}$ resembles the behavior proposed by LaMer [19,20] leading via supersaturation – where nucleation occurs – to an equilibrium between saturated solution and precipitate. Therefore, the

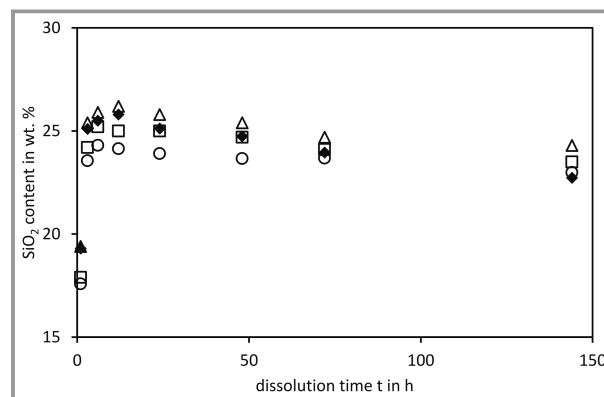


Figure 3. SiO_2 content of liquid water glass produced by hydrothermal dissolution at 160°C as a function of dissolution time t . \circ batch A; \square batch B; \triangle batch C; \blacklozenge batch D.

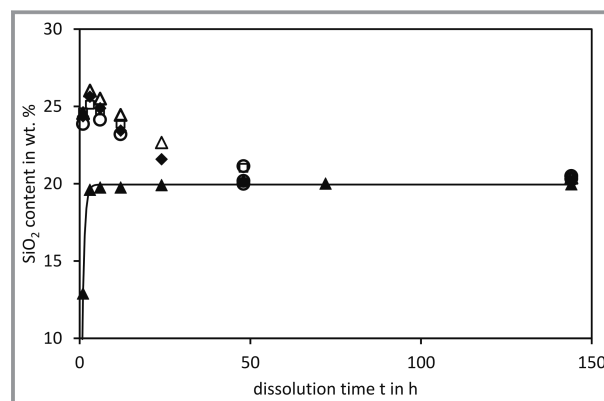


Figure 4. SiO_2 content of liquid water glass produced by hydrothermal dissolution at 200°C as a function of dissolution time t . \circ batch A; \square batch B; \triangle batch C; \blacklozenge batch D; - fit to 100 % quartz data according to numerical simulation in [4].

decrease of SiO₂ content at temperatures between 160 and 220 °C was supposed to be due to crystallization and a new test series with batch C was started to characterize the phase composition of solid residues obtained after longer dissolution times.

A dissolution time of 48 h was applied at temperatures between 100 and 220 °C. The analytical data, composition and some properties, are listed in Tab. 2. The precipitates were characterized by XRD. Amorphous silica (at 100 °C, but not at higher temperatures), low cristobalite (100, 130 and 160 °C; RRUFF powder diffraction file R060648 [23]), and low quartz (all temperatures; RRUFF data base [23]: R110108) were found in the precipitates. Tab. 2 includes intensities of two typical peaks for low cristobalite and low quartz. The peak intensities give semiquantitative information on phase composition. The XRD results for the precipitates obtained at 100 °C and at 200 °C are shown in Fig. S3 (SI). At 100 °C a small amorphous peak at 20–25° 2θ (CuKα radiation), a peak at 20.9° 2θ (attributed to (100) of low quartz), and a peak at 22.1° 2θ (attributed to (101) of low cristobalite) were observed.

In the precipitate obtained at 200 °C only the low quartz peak in that scattering range was found. The intensity of the low cristobalite peak had its maximum at 130 °C, declined distinctly at 160 °C, and was absent at 200 and 220 °C. The peak maxima shifted with higher temperatures slightly towards lower diffraction angles (20.93° at 100 °C and 20.78° at 220 °C), indicating a lower X-ray density of the low quartz obtained at higher temperatures. This can be explained with the assumption that the low quartz found in the residue is a newly crystallized phase and not a remnant of the dissolving material. It should be noted that the peak intensities measured for the 100 °C precipitate are much lower than the peak intensities of the 200 °C precipitate. This difference is due to the amorphous phase in the 100 °C precipitate, which indicates that the QN-D50 powder had not fully reacted within 48 h at 100 °C. The absence of an amorphous halo at 130 °C shows that at this temperature the reaction of QN-D50 powder was almost complete and

the precipitate consisted of newly formed phases. The occurrence of low quartz in the 100 °C and 130 °C precipitates is not only due to contaminations of the starting material but indicates that low quartz might be an equilibrium phase already at these temperatures. The formation of low cristobalite then might be due to Ostwald's step rule. The other physical or chemical parameters like pH, refractive index, density, and viscosity are in good agreement with published data [2, 25].

3.3 Data Analysis

The analytical results obtained at 100 and 130 °C (Tab. S2) were evaluated with an iterative calculation procedure described in [4]: Starting with the particle size distribution of QN-D50 (Tab. S1) the radius of the particles, which were assumed to be spherical, were reduced with an initial dissolution rate $q_{diss,1}$. The volume of the dissolved particle shell was used to calculate the actual dissolved SiO₂ concentration $c_{a,u}$ (for the u -th iteration step). The iterative contribution of each dissolved particle shell was added to the mass of dissolved SiO₂. The dissolution rates were then reduced with a term according to the Noyce-Whitney law:

$$q_{diss,u+1} = q_{diss,u} \left(1 - \frac{c_{a,u}}{c_{\infty,NW}} \right) \quad (4)$$

By optimizing $q_{diss,1}$ and $c_{\infty,NW}$ the calculated SiO₂ contents ($c_{a,u}$) are fitted to the experimentally determined SiO₂ concentrations with a least square method. The optimized data are listed in Tab. S5. The accuracy of the calculation method is estimated as ± 0.2 wt %. In Fig. 2 the experimental data for hydrothermal dissolution of batch A are compared to the fit. At 160 °C the concentration of SiO₂ decreases at longer dissolution times. Nevertheless, the first data points allowed to calculate $c_{\infty,NW}$ and $q_{diss,1}$ even at that temperature. At temperatures ≥ 200 °C that calculation was not applicable, since the SiO₂ contents decreased with time too early. Thus, not enough data points were available to

Table 2. Composition and properties of liquid sodium water glasses and precipitates obtained for batch C; dissolution time 48 h, dissolution temperature reported in this table; information on accuracy also in this table.

T [°C]	100	130	160	200	220
SiO ₂ [wt %] (± 0.2 wt %)	19.5	25.0	24.4	20.7	19.5
Na ₂ O [wt %] (± 0.1 wt %)	–	7.6	7.5	7.9	7.8
R_m	–	3.34	3.36	2.70	2.58
pH (± 0.05)	11.38	11.26	11.26	11.72	11.77
Refractive index n (± 0.005)	1.372	1.384	1.383	1.382	1.380
Density ρ [g cm ⁻³] (± 0.003 g cm ⁻³)	1.238	1.322	1.309	1.284	1.272
Viscosity η [dPa s] (± 2 dPa s)	5.8	25.1	18.1	7.9	6.7
Intensity of (101) of low cristobalite [cps]	700	2000	1000	n. d.	n. d.
Intensity of (100) of low quartz [cps]	810	3000	2160	3550	2700

calculate $q_{diss,1}$ and $c_{\infty,NW}$ for the period where the SiO_2 content increases. Since $c_{\infty,NW}$ was not available for 200 and 220 °C, the highest SiO_2 contents c_{max} reached intermediately are listed in Tab. S5. These SiO_2 contents are almost as high as the optimized $c_{\infty,NW}$ values calculated for lower temperatures. c_{max} is regarded as slight underestimation of the theoretical maximum, which might be up to 0.5 wt % higher. The dependence of these SiO_2 contents ($c_{\infty,NW}$ at 100–160 °C and c_{max} at 200 and 220 °C) is shown in Fig. 5 as a function of dissolution temperature. The c_{max} values even of batch D are higher than the solubilities of low quartz reported in [4]. The differences between $c_{\infty,NW}$ and the c_{max} values of the four batches cover a range between 24 and 26 wt % and seem to be more dependent on batch type than on dissolution temperature. Therefore, the cause of these limitation shown at least to exist at 100 and 130 °C has to be questioned.

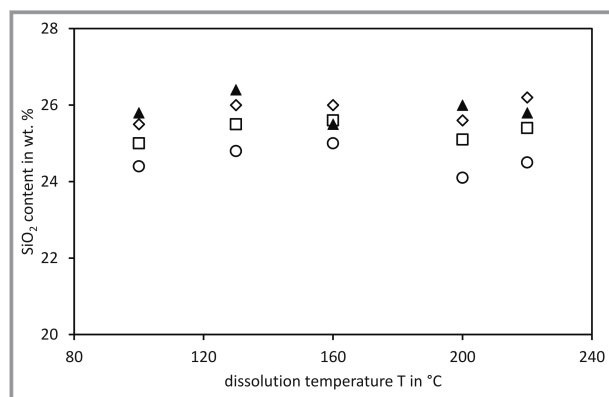


Figure 5. SiO_2 contents $c_{\infty,NW}$ (100 °C to 160 °C) and c_{max} (200 °C and 220 °C) achieved with batches A (○), B (□), C (▲), and D (◇) as a function of dissolution temperature T .

The time dependence of the SiO_2 content at longer times during crystallization at 160, 200, and 220 °C was evaluated according to a first order reaction [26]:

$$-\frac{dc_a}{dt} = k(c_{\infty,c} - c_a) \quad (5)$$

The reaction described here has some deviations from standard conditions. Here, the concentration of SiO_2 is evaluated, which starts at an unknown value and approaches a final concentration > 0 . Therefore, k is derived from a plot of $\ln(c_a/(c_a - c_{\infty,c}))$ vs. t . At 160 °C the crystallization rate was quite slow. Therefore, additional test runs with a dissolution time of 672 h (= 28 d) were made. The concentration dependence on time derived from that plot is shown in Fig. S4 (SI) according to the following equation:

$$c_a = A_0 \exp(-kt) + c_{\infty,c} \quad (6)$$

The calculated data of $c_{\infty,c}$ and k are included in Tab. S5. The values of $c_{\infty,c}$ are nearly equal to the solubilities of SiO_2 in equilibrium with low quartz reported in [4]. These data

are included in Tab. S5 and in Fig. 6, too. At 200 and 220 °C the c_{max} values even of batch D are higher than the $c_{\infty,c}$ values. This shows that additional seeding does not avoid oversaturation. To avoid oversaturation higher low quartz contents of the batch are needed.

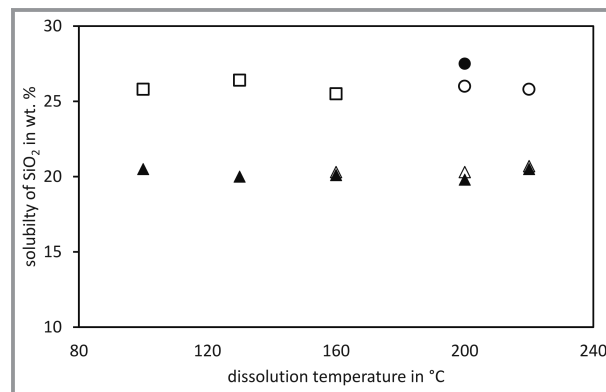


Figure 6. Final SiO_2 contents as function of dissolution temperature T ; □ $c_{\infty,NW}$ calculated according to [4] for QP-DN50 (batch C); ○ c_{max} for QP-DN50 (batch C); ● literature data reported by Rowe et al. [27]; ▲ $c_{\infty,NW}$ reported in [4] for low quartz; △ $c_{\infty,c}$ (Tab. S5, at 160 and 220 °C identical with ▲).

4 Summary and Discussion

The following findings can be reported for the respective dissolution temperatures:

- 100 °C: The SiO_2 contents of the liquid sodium water glasses approximated final values of about 24–26 wt %, depending on batch type. Neither oversaturation nor decline of SiO_2 content due to crystallization was observed. The precipitate contained cristobalite as new phase and an amorphous phase as remnant of the starting materials.
- 130 °C: Essentially the same behavior as at 100 °C was observed. In the precipitate, no amorphous phase was detected, which shows that the starting material nearly fully reacted and the precipitate being a new phase.
- 160 °C: The SiO_2 content passes a maximum but declines at longer dissolution times. The decline is due to the crystallization of low quartz. The kinetics of crystallization at this temperature are quite slow so that the final value $c_{\infty,c}$ is not reached within 28 d.
- 200 °C: The SiO_2 content passes a maximum but declines within a few days to a final value $c_{\infty,c}$, which is identical to the solubility of low quartz dissolved under the same conditions [4]. These results are typical of oversaturation (LaMer type).
- 220 °C: The highest SiO_2 contents are reached within 1 h of dissolution. Then the SiO_2 contents approach the final value $c_{\infty,c}$, again identical to the solubility limit of low quartz.

The dissolution kinetics of the technical grade vitreous silica QP-DN50 applied here shows two temperature

regimes. At 100 and 130 °C the SiO₂ content of the liquid sodium water glasses approached a final limitation called c_{∞} . This limitation changed to a certain degree with the type of batch for up to 2 wt % SiO₂ content. The higher the SiO₂ content of the batch, the higher c_{∞} . The short time results obtained at 160 ° were extrapolated according to the iterative calculation method presented in [4]. The existence of cristobalite in the precipitate shows that the concentration of SiO₂ does not approach an equilibrium solubility of vitreous silica, but possibly one of low cristobalite. It is assumed that at these low temperatures the crystallization of low quartz is either restricted due to very low crystallization rates or due to kinetic barriers.

At temperatures ≥ 160 °C the SiO₂ content declined after reaching a maximum. The precipitate contains low quartz as main phase. As the SiO₂ contents approach $c_{\infty,c}$ values identical to the solubility limits of low quartz it is concluded that this is the equilibrium phase at these temperatures.

A calculation of $c_{\infty,NW}$ according to the iterative modeling was not possible for results obtained at 200 and 220 °C. Here the maximum SiO₂ contents reached after short times are close to $c_{\infty,NW}$ derived for lower temperatures. At temperatures ≥ 160 °C the SiO₂ content declined after reaching a maximum and approached a long-term limitation called $c_{\infty,c}$. These $c_{\infty,c}$ values are almost identical to the solubility limits obtained for low quartz in [4]. This was confirmed by phase analysis of the precipitates of the dissolution processes: at temperatures of 100 and 130 °C low cristobalite was found, whereas at higher temperatures only low quartz was identified. Low cristobalite is a new phase formed at 100 and 130 °C. Low quartz was already detected in small amounts in the starting material QP-DN50. There are two possibilities: either low quartz impurities of QP-DN50 act as seeds, which grew predominantly at temperatures ≥ 160 °C, or additional seeding and crystal growth occurred at these temperatures. The addition of small amounts of low quartz to batch D did not change the dissolution or crystallization behavior during the test runs.

As an example, the $c_{\infty,NW}$ and the c_{∞} values obtained for batch C are shown in Fig. 6. They are compared with solubilities of low quartz reported in [4] and some data derived from a publication of Rowe et al [27]. Additionally, the $c_{\infty,c}$ values of Tab. S5 are included. They are almost identical with the low quartz solubilities reported in [4]. The value of Rowe et al. fits to the c_{max} values of batch C. Since they used crystalline sodium silicates and not quartz as raw materials, they probably avoided quartz crystallization successfully. The $c_{\infty,NW}$ and c_{max} values determined in dissolution tests with QN-D50 are probably solubility limits of cristobalite, which was found in precipitates after 48 h at 100 to 160 °C. On the other hand, $c_{\infty,NW}$ and c_{max} depended to a certain degree – up to 2 wt % SiO₂ content – on the type of batch. This finding possibly contradicts a solubility limitation. Whether other dependencies – like increase of viscosity due to increasing water glass concentration – are able to produce concentration limitations has to be investigated further. The

$c_{\infty,NW}$ values determined in dissolution tests with low quartz were interpreted as solubility limit of low quartz. Both solubility limits seem to be independent on temperature between 100 and 220 °C. The kinetics controlling dissolution at low temperatures (100 and 130 °C, and during short times at 160 °C) seem to be equal to those derived for low quartz [4]: the dissolution rate is proportional to the exposed surface area and lowered by a concentration dependence according to the Noyce-Whitney law [20]. One interesting further result is that the increasing the SiO₂ content of the batch reduces the dissolution rate $q_{diss,i}$.

The temperature dependence of the dissolution kinetics was evaluated according to Arrhenius. It is a thermally activated reaction, and the results are shown in Fig. 7 as natural logarithm of the dissolution rate vs. reciprocal temperature. The data for QP-DN50 are compared to the dissolution rates obtained for low quartz [4]. For the low quartz data an activation energy of 75 ± 5 kJ mol⁻¹ was reported. If mean values for the dissolution rates for all four batches (Tab. S5) are evaluated the activation energy of QP-DN50 dissolution is 28 ± 5 kJ mol⁻¹. At about 200 °C dissolution rates of low quartz or vitreous silica will become equal if those of vitreous silica are extrapolated.

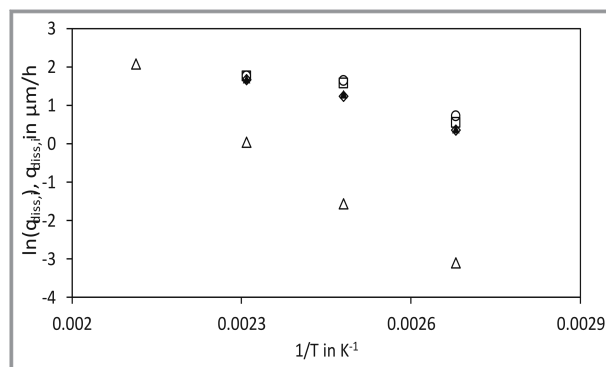


Figure 7. Natural logarithm of the initial dissolution rate $q_{diss,i}$ vs. reciprocal temperature; ○ batch A, □ batch B, ▲ batch C, ◇ batch D, △ low quartz (Dörentrup W6).

The crystallization of low quartz was also evaluated with respect to thermal activation. The k values obtained for tests at 160–220 °C according to Eq. (6) have been evaluated. The data are listed in Tab. S5. The mean activation energy of batches A, B, C was 120 ± 20 kJ mol⁻¹. The seeded batch D had an activation energy of about 100 kJ mol⁻¹. Laudise [28] reported an activation energy for the crystallization of low quartz in 0.5 M NaOH at 300–400 °C of 92 kJ mol⁻¹. He stated also that growth kinetics and activation energies depend on crystallographical growth direction with activation energies ranging from 60 to 170 kJ mol⁻¹. Since Laudise used oriented seed crystals of low quartz – his studies were made in the context of growing single crystals – the mean value of 92 kJ mol⁻¹ is quite close to the value of 100 kJ mol⁻¹ obtained for batch D in this study.

According to thermodynamic data and phase diagrams [6] it is expected that low quartz is the equilibrium phase also at 100 and 130 °C. But it is possible that crystallization of this phase is hindered or delayed kinetically at these temperatures.

5 Conclusion

Dissolution of vitreous silica in NaOH lyes is more complex than dissolution of low quartz at the same conditions. At 100 and 130 °C the SiO₂ contents increase with time and reach a constant value. The kinetics of dissolution at these temperatures are governed by exposed surfaces area and reduced by SiO₂ saturation according to a Noyce-Whitney law. But the precipitate contains low cristobalite as a new phase. Therefore, it is not an equilibrium between vitreous silica and liquid sodium water glass. Possibly, low cristobalite is the equilibrium phase at 100 and 130 °C, but it is more likely that low quartz is the equilibrium phase and the occurrence of low cristobalite is due to Ostwald's step rule. But the final $c_{\infty,NW}$ values represent then a metastable equilibrium between low cristobalite and liquid sodium water glass. At temperatures ≥ 160 °C SiO₂ concentration passes high values close to the maximum values (c_{max}) obtained at lower temperatures and decline then to the equilibrium solubilities of low quartz. This concentration dependence resembles a LaMer-type [19] behavior. The liquid sodium water glass is temporarily oversaturated with respect to low quartz but not to low cristobalite. The c_{max} values obtained intermediately can eventually be taken as a slightly lower limit of cristobalite solubility.

The dissolution rate of vitreous silica QP-DN50 is less temperature dependent than that of low quartz. They should become equal at about 200 °C. The technological consequences of the findings presented here are that it should be possible to dissolve vitreous silica to liquid sodium water glasses with $R_m \geq 3.3$ and a SiO₂ content ≥ 25 wt %. At low temperatures (e.g., 100 °C) long dissolution times are needed, at high temperature (e.g., 200 °C) an online monitoring of SO₂ concentration should help to prevent crystallization of low quartz. Then short dissolution times should be possible.

Supporting Information

Supporting Information for this article can be found under DOI: <https://doi.org/10.1002/cite.202000107>.

The experimental help of members of the working group Anorganisch-Nichtmetallische Materialien (inorganic-nonmetallic materials) of the Institute of Physics of the Martin-Luther-Universität Halle-Wittenberg and of E. Koslowski (X-ray diffraction, Institute of Chemistry, same university), is gratefully acknowledged. Open access funding enabled and organized by Projekt DEAL.

Symbols used

c_a	[wt %]	actual silica concentration
$c_{a,u}$	[wt %]	actual silica concentration after $u \times \Delta t$
$c_{\infty,NW}$	[wt %]	final silica concentration according to Noyce-Whitney law [19]
$c_{\infty,c}$	[wt %]	final SiO ₂ content due to crystallization
c_{max}	[wt %]	highest measured SiO ₂ content in a test series at constant temperature
d_i	[μm]	mean diameter of size class i
d_{50}	[μm]	midpoint value: particle size at which 50 wt % of the particles are smaller
k	[h^{-1}]	rate constant
m_i	[g]	mass of particles of size class i
n	[–]	refractive index
$q_{diss,1}$	[$\mu\text{m h}^{-1}$]	initial dissolution rate
$q_{diss,u}$	[$\mu\text{m h}^{-1}$]	dissolution rate of u -th time step
R_m	[–]	molar SiO ₂ :Na ₂ O ratio
t	[h]	time
T	[°C]	temperature
u	[–]	number of time steps in iteration

Greek letters

η	[dPa s]	viscosity
λ	[nm]	wavelength
θ	[°]	diffraction angle

Abbreviations

aq.	aqueous (dissolved in H ₂ O)
cps	counts per second
d	day
DLVO	Derjaguin, Landau, Verweij, Overbeek (authors first describing the DLVO theory)
liq.	liquid
n. d.	not detected
PFA	perfluoro alkoxy alkanes
PTFE	polytetrafluoro ethylene
RSC	residual solids content
s	solid
XRD	X-ray diffraction

References

- [1] H. H. Weldes, K. R. Lange, *Ind. Eng. Chem.* **1969**, *61*, 29–44.
- [2] H. Roggendorf, W. Grond, M. Hurbanic, *Glass Sci. Technol.* **1996**, *69*, 216–231.
- [3] R. Novotny, J. Schürtz, *Patent DE 3902751 A1*, **1990**.
- [4] T. Pfeiffer, S. A. H. Sander, D. Enke, H. Roggendorf, *Chem. Ing. Tech.* **2019**, *91*, 92–101.
- [5] T. Pfeiffer, D. Enke, R. Roth, H. Roggendorf, *Adv. Chem. Eng. Sci.* **2017**, *7*, 76–90.
- [6] R. K. Iler, *Chemistry of silica*, Wiley-Interscience, New York **1979**.

- [7] W. Stöber, *Beitr. Silikose-Forsch.* **1966**, 89, 1–113.
- [8] I. Gunnarsson, S. Arnorsson, *Geochim. Cosmochim. Acta* **2000**, 64, 2295–2307.
- [9] J. S. Falcone, J. L. Bass, P. H. Krumrine, K. Brensinger, E. R. Schenk, *J. Phys. Chem. A* **2010**, 114, 2438–2446.
- [10] J. D. Rimstidt, H. L. Barnes, *Geochim. Cosmochim. Acta* **1980**, 44, 1683–1699.
- [11] W. Stumm, *Aquatic chemistry*, Wiley-Interscience, New York **1970**.
- [12] K. R. Andersson, L. S. Dent Glasser, D. N. Smith, in *Soluble silicates* (Ed: J. S. Falcone), American Chemical Society, Washington DC **1982**, 115–131.
- [13] R. K. Iler, in *Soluble silicates* (Ed: J. S. Falcone), American Chemical Society, Washington DC **1982**, 95–114.
- [14] D. Böschel, M. Janich, H. Roggendorf, *J. Colloid Interface Sci.* **2003**, 267, 360–368.
- [15] B. Derjaguin, L. Landau, *Progr. Surf. Sci.* **1993**, 43, 30–59.
- [16] T. W. Healy, in *The colloidal chemistry of silica* (Ed: H. C. Bergna), American Chemical Society, Washington DC **1994**, 147–159.
- [17] J. L. Bitter, G. A. Duncan, D. J. Beltran-Villegas, D. H. Fairbrother, M. A. Bevan, *Langmuir* **2013**, 29, 8835–8844.
- [18] P. M. Dove, D. A. Crerar, *Geochim Cosmochim. Acta* **1990**, 54, 955–969.
- [19] V. K. LaMer, *Ind. Eng. Chem.* **1952**, 44, 1270–1277.
- [20] A. A. Noyes, W. R. Whitney, *J. Am. Chem. Soc.* **1897**, 19, 930–934.
- [21] R. Brückner, *J. Non-Cryst. Sol.* **1970**, 5, 123–170.
- [22] I. G. Polyakova, in *Glass – selected properties and crystallization* (Ed: J. P. Schmelzer), W. De Gruyter, Berlin **2016**, 197–267.
- [23] B. Lafuente, R. T. Downs, H. Yang, N. Stone, in *Highlights in Mineralogical Crystallography* (Eds: T. Armbruster, R. M. Danisi), W. De Gruyter, Berlin **2015**, 1–30.
- [24] L. Levien, C. T. Prewitt, D. J. Weidner, *Am. Mineral.* **1980**, 65, 920–930.
- [25] J. G. Vail, *Soluble silicates - their properties and uses. Vol. 1, Chemistry*. Reinhold Publishing, New York **1952**.
- [26] W. J. Moore, *Physical Chemistry*. Longman Publishing Group, London **1998**.
- [27] J. J. Rowe, R. O. Fournier, G. W. Morey, *Inorg. Chem.* **1967**, 6, 1183–1185.
- [28] R. A. Laudise, *J. Am. Chem. Soc.* **1959**, 81, 562–566.